Acquiring 4D CT data for Monte Carlo calculations

Paul Keall[1,2] and Kristy Brock[3]

[1]Stanford University

[2]Virginia Commonwealth University

[3]Princess Margaret Hospital

Potential conflicts-of-interest

- I am PI of a sponsored research agreement between Stanford and Varian Medical Systems

Educational objectives

- Understand the mechanism and application of 4D CT imaging
- Understand the central role of deformable image registration in 4D dose calculations
- Understand a framework for 4D dose calculation

Introduction

- Accuracy of MC is limited by:
  - Input radiation source description
  - Accuracy of input geometry and materials
  - Physical processes modeled
  - Cross-sections
- This talk focuses on the patient geometric input, particularly the acquisition and use of time dependent CT images

Introduction

- Formalism developed for intrafraction respiratory motion but can be extended for interfraction adaptive radiotherapy
- Use of MC for 4D anatomic calculations is relatively new, however likely to increase in importance
  - 4D data more available
  - MC more available
  - Deformable image registration algorithms more available
  - Adaptive radiotherapy schemes becoming more available
- Overall desire to estimate the radiation dose as accurately as possible

Input requirements for 4D MC calculations

- 4D CT-capable scanner to create anatomic input
- Deformable image registration algorithm
- 4D-capable treatment planning system
- Commissioned Monte Carlo system

4D Monte Carlo flowchart

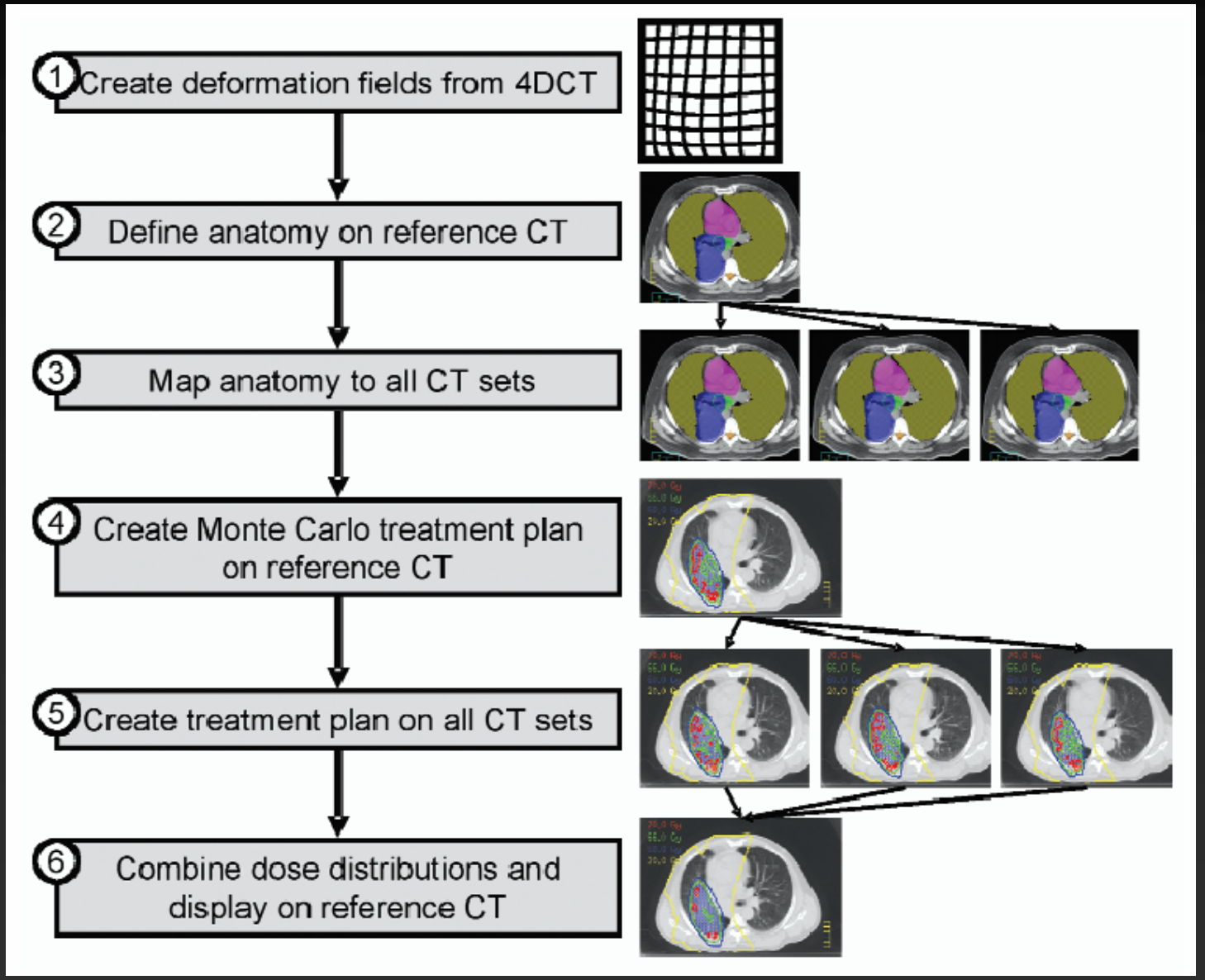

4D CT Imaging

4D thoracic CT imaging

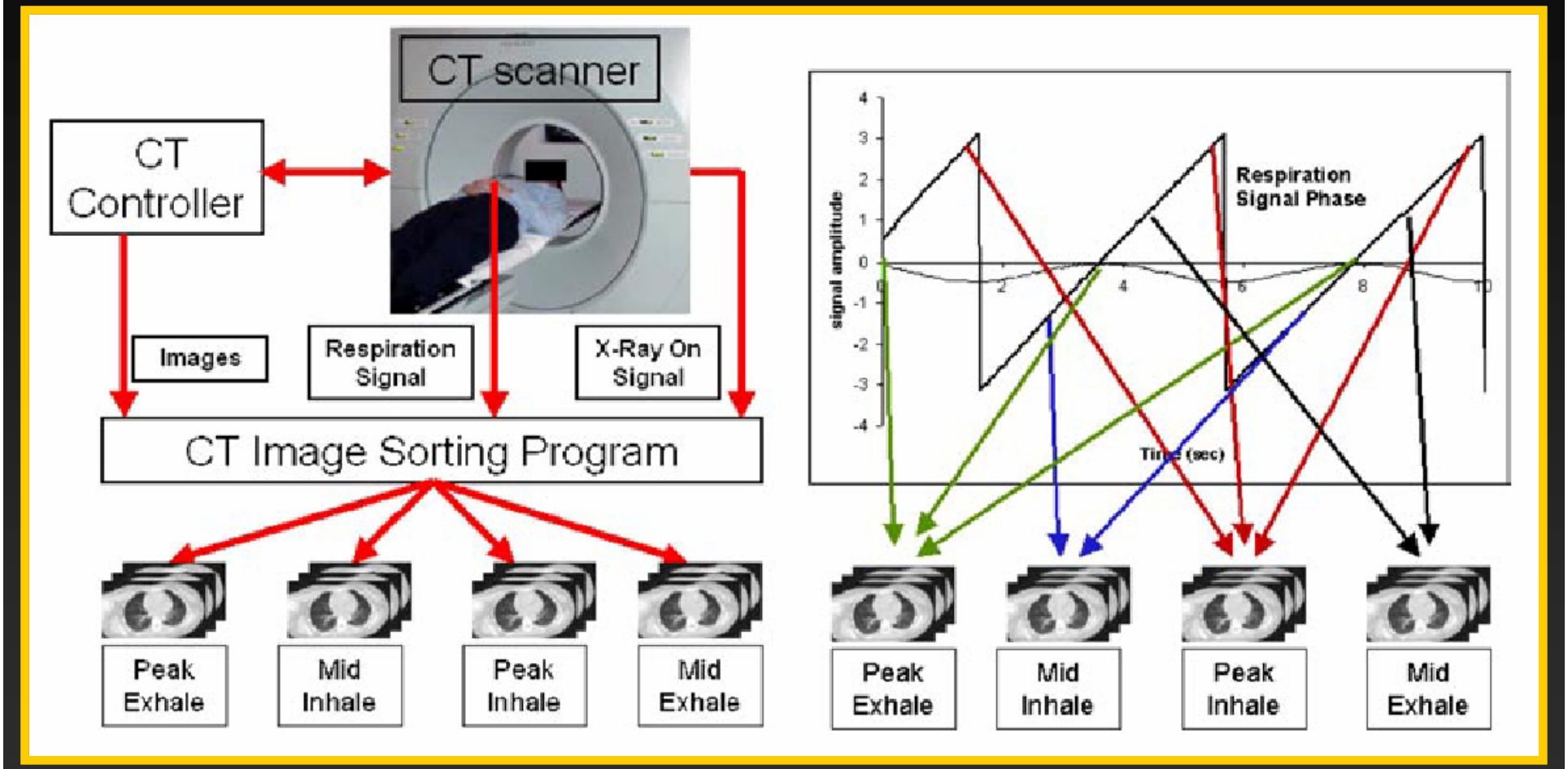

Vedam *et al* PMB 2003

What use are 4D CT scans?

- Determine tumor motion/screening
- Motion inclusive treatment
- Respiratory gated treatment
- 4D radiotherapy

4D CT imaging can be

- Ciné or helical acquisition
- Sinogram or image sorting
- Input signal can come from many sources
- Patient is limiting factor!

Brief history of 4D thoracic CT

Development	Year	First Author	Institution
Single slice helical	2003	Ford, Vedam	MSKCC, VCU
Multislice cine (commercial)	2003	Pan (2004)	GE/MGH/MSKCC
Cone beam (benchtop)	2003	Taguchi	Toshiba
Multislice cine	2003	Low	Washington University
Multislice helical	2004b	Keall	VCU, MDACC
Multislice cine PET/CT	2004a,b	Nehmeh	MSKCC
Cone beam (clinical)	2005	Sonke	NKI
Applications outside radiation oncology	2005-present	Guerrero, Keall[1], Low	MDACC, VCU, Washington University

4D CT images

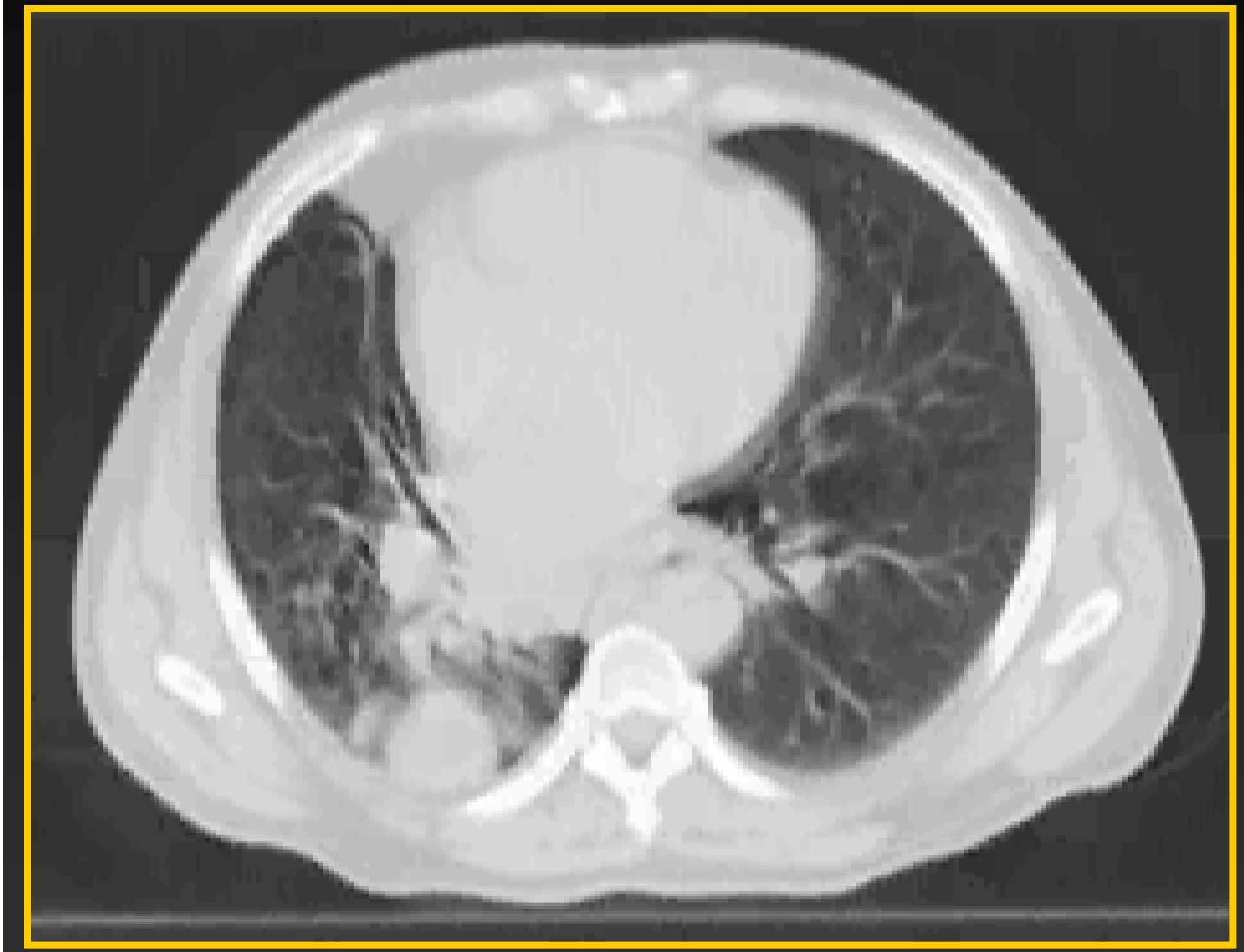

Vedam *et al* PMB 2003 48:45-62

8 respiratory phases
- Peak inhale
- Early inhale
- Mid inhale
- End inhale
- Peak exhale
- Early exhale
- Mid exhale
- Late exhale

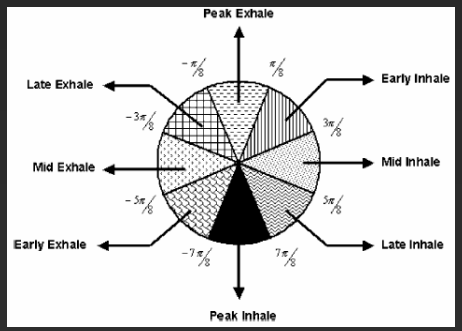

Respiratory variability

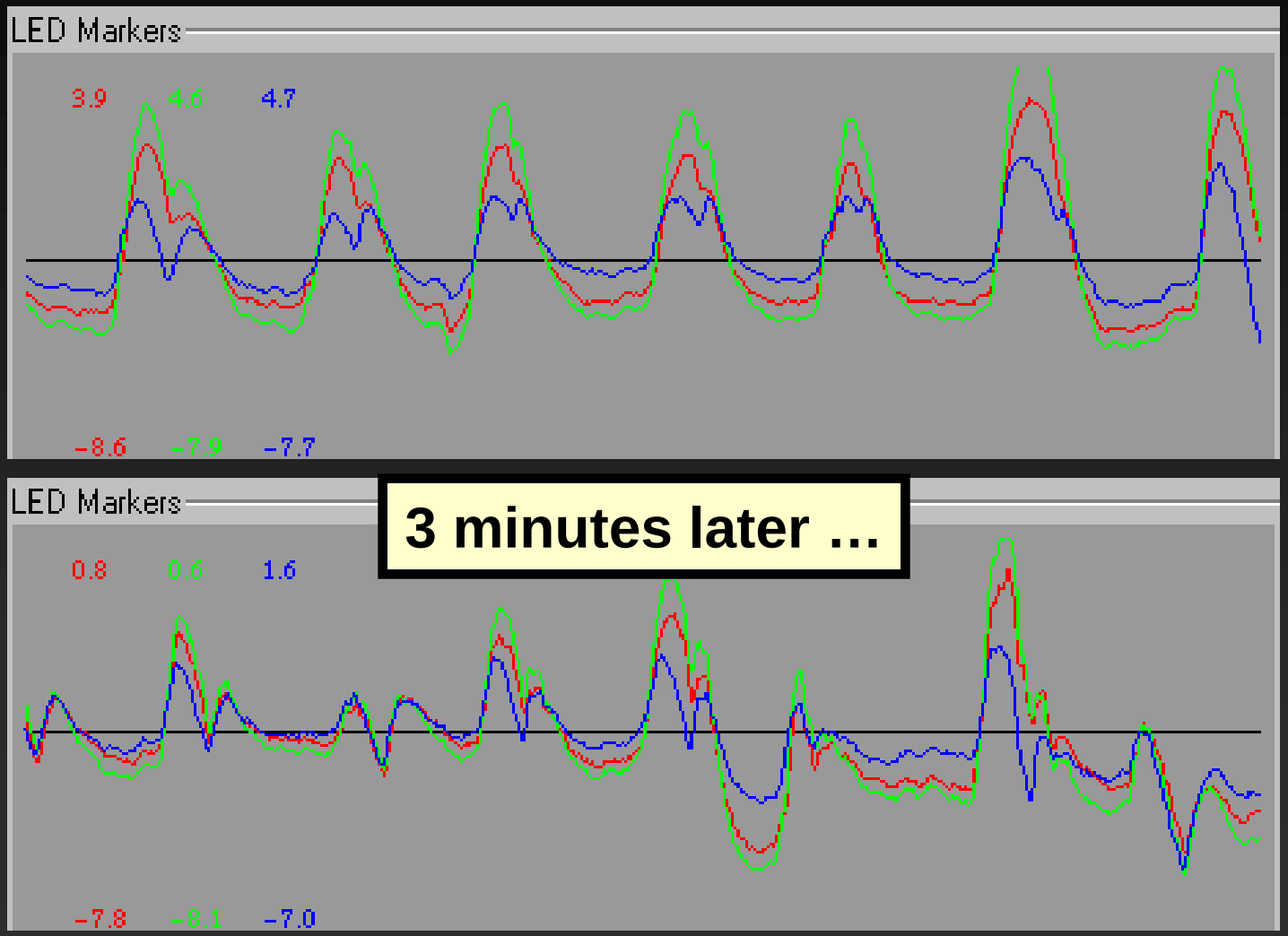

Courtesy Sonja Dieterich, Georgetown University

What 4D MD CT is available?

Vendor	Respiratory signal	Ciné/Helical	Reconstruction Options	When Available?
GE	Varian RPM Optical	Ciné	Image sorting based on displacement or phase of signal	FDA approved
Philips	Varian RPM Optical + Bellows	Helical	Sinogram sorting based on respiratory "tags"	FDA approved
Siemens	Abdominal belt	Helical	Sinogram sorting based on respiratory waveform	FDA approved
Toshiba	Abdominal belt	Ciné	Image sorting based on respiratory waveform	Spring 2006 (256 row)

Cone beam CT

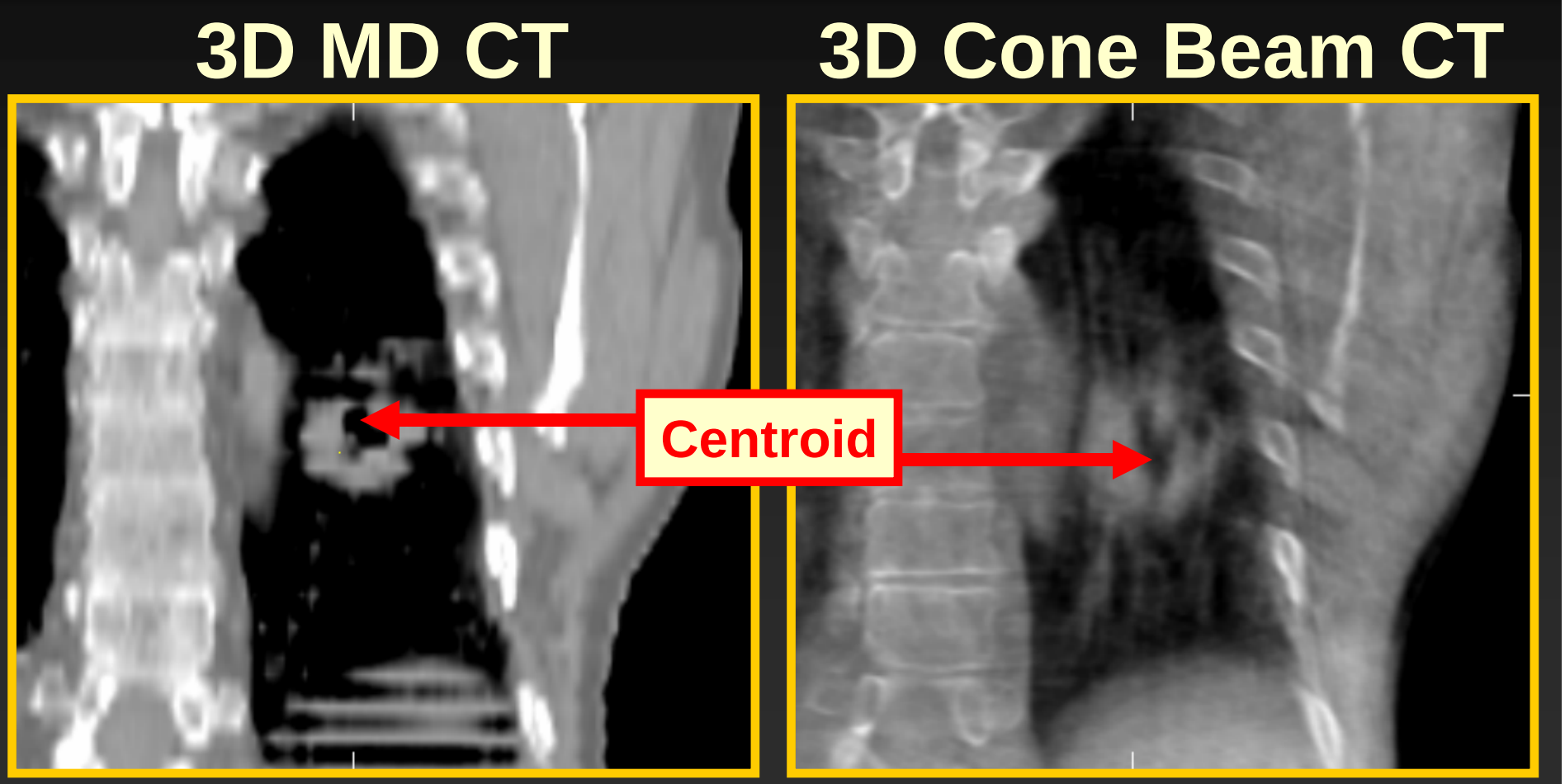

Courtesy Sonke *et al* Med Phys 2005

4D cone beam CT

Courtesy Sonke *et al* Med Phys 2005

Deformable image registration

Deformable image registration

- Non-rigid registration algorithms
- Map objects/pixels in one image to another
- Create a displacement vector field (DVF)
- Characterized by similarity metric and interpolation method

Deformable image registration

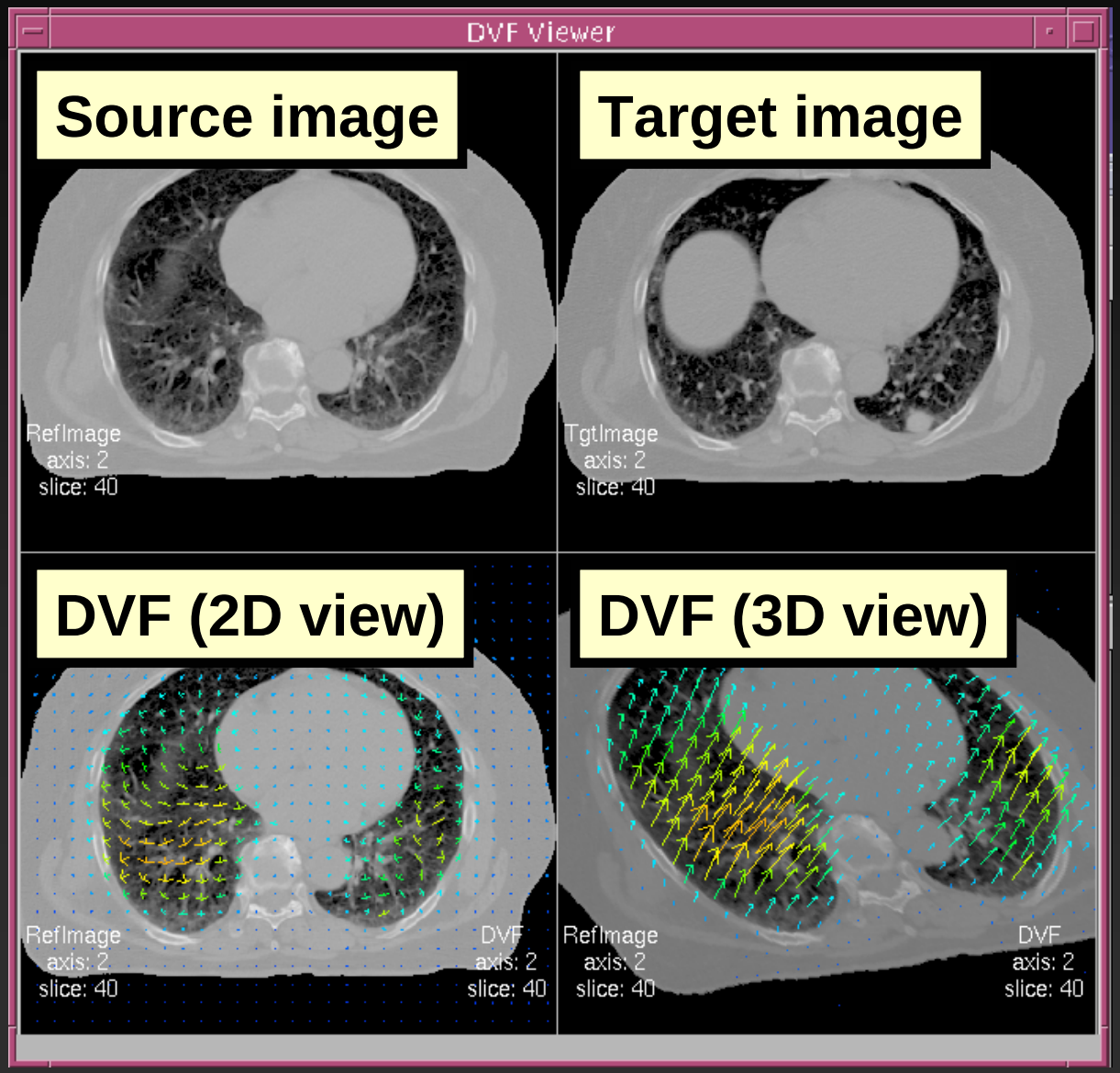

Similarity metric and interpolation methods

Similarity Metric	Interpolation Method
Mutual information	Viscous fluid velocity field
Cross correlation	Optical flow
Minimum mean squared difference	Thin plate spline
Contour matching	B-spline
	Finite element analysis

Finite element analysis

The fundamental equation of finite element analysis (FEA) for an elastic body is given by Hooke's Law, shown in Equation (6),

$$\mathbf{K}\mathbf{u} = -\mathbf{F}, \tag{6}$$

where K is the stiffness matrix of the elastic material, **u** is the displacement vector, and **F** is the applied force. Equation (6) is solved by specifying boundary conditions, defined through forces or set displacements on a subset of the nodes in the finite element model. A finite element model is a series of connected points, or nodes, that when combined together to form a mesh, describe a volume of interest. The imple-

Large deformation diffeomorphic image registration

et al. 2005). The viscous-fluid, ordinary differential equation is given by Equation (7),

$$\frac{d\mathbf{u}(\mathbf{x},\theta)}{d\theta} = v\left(\mathbf{u}(\mathbf{x},\theta),\theta\right), \tag{7}$$

where $v(\mathbf{u},\theta)$ is the velocity field. The deformation field is solved by maximizing a similarity metric while constraining the deformation field to comply with the laws of continuum mechanics, resulting from viscous-fluid modeling using the Navier–Stokes equations on the velocity fields.

Optical flow

Optical flow is described by Equation (8),

$$\mathbf{u} = \frac{\left[I(\mathbf{x},\theta_k) - I(\mathbf{x},\theta_0)\right]\nabla I(\theta_0)}{\left|\nabla I(\theta_0)\right|^2 + \left[I(\mathbf{x},\theta_k) - I(\mathbf{x},\theta_0)\right]^2}, \tag{8}$$

and $\mathbf{u} = (u_x, u_y, u_z)$, $\vec{\nabla} I(\theta_0)$ is the gradient of the static image. The difference in the image intensity in the two images and the gradient of the static image, external and internal forces, respectively, act as competing forces, since the algorithm is optimized to minimize both. This algorithm was implemented by Thirion in the "demons" algorithm through an iterative process of solving Equation (8) and regularizing the deformation field using a Gaussian filter to smooth the deformation field (Thirion 1998). Wang et al. (2005a,b) have recently added active forces, based on the gradient of the moving image, to the demons algorithm to improve efficiency of registration, resulting in Equation (9).

$$\mathbf{u} = \left(I(x,\theta_k) - I(x,\theta_0)\right) \times \left(\frac{\vec{\nabla} I(\theta_0)}{\left|\nabla I(\theta_0)\right|^2 + \left(I(x,\theta_0) - I(x,\theta_k)\right)^2} + \frac{\nabla I(\theta_k)}{\left|\nabla I(\theta_k)\right|^2 + \left(I(x,\theta_0) - I(x,\theta_k)\right)^2} \right) \tag{9}$$

Splines: Thin plate and b

Spline interpolation techniques use a grid of control points, or "knots," to deform the image. The use of thin plate splines (TPS) was introduced by Bookstein (1989) to model biological shape changes such as deformation. The more knots, the more degrees of freedom the registration has, and each knot has a global effect on the entire image. TPS is based on the fundamental solution to the biharmonic equation,

$$f(x,y,z) = |r|, \tag{10}$$

where $r = \sqrt{x^2 + y^2 + z^2}$.

Hierarchical B-splines, which were first described by Forsey and Bartels (1988), consist of piecewise polynomial basis functions that affect only a local area of the image. A tricubic B-spline is defined in Equation (11), where are the cubic B-spline basis functions and b_{ijk} are the control points or knots in the volume.

$$f(x,y,z) = \sum_{i=0}^{r}\sum_{j=0}^{s}\sum_{k=0}^{t} b_{ijk} N_i^3(x) N_j^3(y) N_k^3(z) \tag{11}$$

The bending energy, which is independent of any affine transformation that the source dataset undergoes, describes the amount of deformation that occurs between two states. Minimization of the bending energy of the perturbation is often used in TPS and B-spline implementation to avoid unrealistic deformations. The bending energy, a positive and unitless number, is defined in Equation (12).

$$I[f(x,y,z)] = \iiint \left(\left(\frac{\partial^2 f}{\partial x^2}\right)^2 + \left(\frac{\partial^2 f}{\partial y^2}\right)^2 + \left(\frac{\partial^2 f}{\partial z^2}\right)^2 + \left(\frac{\partial^2 f}{\partial xy}\right)^2 + \left(\frac{\partial^2 f}{\partial xz}\right)^2 + \left(\frac{\partial^2 f}{\partial yz}\right)^2 \right) dxdydz \tag{12}$$

Calculus of variations

similarity measure and the smoothness constraints applied. The voxels are allowed to move freely and are constrained through the minimization of the energy functional defined in Equation (13),

$$\hat{\mathbf{u}} = \arg\min \varepsilon(\mathbf{u}) \,, \tag{13}$$

where

$$\varepsilon(\mathbf{u}) = \int_{\mathbf{x}\in R^3} \left[R^2(\mathbf{x},\mathbf{u}) + \lambda \sum_{i=1}^{3} \sum_{j=1}^{3} \left(v_j^i\right)^2 \right] dx \text{ and } v_j^i = \frac{\partial \mathbf{u}^i}{\partial \mathbf{x}^j} \,. \tag{14}$$

The deformation field is then calculated by solving the Euler–Lagrange equation, Equation (15), using a finite difference method and a multi-resolution strategy.

$$\lambda \nabla^2 \mathbf{u} - R(\mathbf{x},\mathbf{u}) \frac{\partial R(\mathbf{x},\mathbf{u})}{\partial \mathbf{u}} = 0 \tag{15}$$

Accuracy

- All DIR algorithms have uncertainties
- Very difficult to quantify on population or individual basis
- Error O(mm) that should not be ignored

First Author	Similarity Metric	Interpolation Scheme	Anatomical Site	Accuracy Metric	Accuracy Average (sd) mm
Bharatha et al. (2001)	Contour, surface matching	FEA	Prostate	2 landmarks	1.01, 0.73 (0.56, 0.40)
Brock et al. (2003a)	MI	TPS	Liver	Bifurcations	LR: 1.3(1.0) AP: 1.5(1.2) SI: 1.5(1.4)
Brock et al. (2005)	Contour, guided surface projection	FEA	Liver	Bifurcations	LR: 0.0 (1.4) AP: –1.0 (2.0) SI: 0.2 (1.7)
			Lung		LR: 1.3 (2.2) AP: 3.2 (2.3) SI: 0.5 (2.2)
			Breast/ Stomach/ Kidneys	Contours	LR: 0.3 (1.4) AP: 0.0 (1.6) SI: –0.3 (1.2)
Coselmon et al. 2004	MI	TPS	Lung	Bifurcations	LR: 0.0 (1,7) AP: –0.5 (3.1) SI: 0.4 (3.6)
Keall et al. 2005	Min mean sq error	Viscous fluid	Lung	Bifurcations	<4.0
Lu et al. 2004	E minimization function of intensity difference	Smoothness	Lung Prostate	Balloon phantom Image overlay CC	<1 mm Qualitative CC: 0.98 – 0.99
Rietzel et al. 2005	Sum sq diff	B-spline	Lung	Difference images	Qualitative
Rohlfing et al. 2004	MI	B-spline	Liver	Surface Landmarks	4.0 2.7
Schaly et al. 2005	Contour	TPS	Prostate	Markers	3.0 (1.9)
Venugopal et al. 2005	Contour	TPS	Prostate	Volume overlap	97%
Wang et al. 2005b	CC or MI	Optical flow + active force	Prostate	Sim. defm Defm. phantom	0.5 (1.5) 0.8 (0.5)
Zhang et al. 2004	Contour, E minimization	FEA	Lung	Image overlay	Qualitative

4D dose computation framework

General framework: 3D and 4D

In 3-D radiotherapy planning, the estimated prescribed dose, D_{Rx} is that computed on the anatomic space x given the anatomy $I(\mathbf{x})$ and beam fluence Ψ,

$$D_{Rx} = D_{Rx}\left(\mathbf{x}\middle|\Psi, I(\mathbf{x})\right). \tag{16}$$

When accounting for intrafraction changes over time t, the estimated prescribed dose is computed on a changing anatomy, $I(\mathbf{x},t)$. The beam fluence $\Psi(t)$ will in general be time dependent. In order to correctly integrate the dose for a given voxel, the time-dependent displacement vector field (DVF) from the DIR algorithm is also needed. Thus, the 4-D estimated prescribed dose is:

$$D_{Rx} \int_{\text{Image start}}^{\text{Image end}} d_{Rx}\left[\mathbf{x}+\mathbf{u}(\mathbf{x},t)\middle|\Psi(t), I(\mathbf{x},t)\right]dt \ , \tag{17}$$

General framework: discrete 4D

However, since the 4-D CT is discrete rather than continuous in time, Equation (17) is approximated by

$$D_{Rx} = \sum_{\text{Phase } k=1}^{P} \lambda_{Rx}^{k} d_{Rx}\left[\mathbf{x} + \mathbf{u}\left(\mathbf{x},\theta_k\right)\middle|\Psi_k, I\left(\mathbf{x},\theta_k\right)\right], \qquad (18)$$

where λ_{Rx}^{k} is a weight term accounting for variations in time spent in each discrete part of the respiratory cycle. The implications of this approximation are discussed in

General framework: 4D delivery

During treatment delivery, the respiratory signal and anatomy (and also potentially beam fluence) will vary from that planned, and thus the delivered dose D_{Tx}^{i} for a given fraction is:

$$D_{Tx}^{i} = \sum_{\text{Phase } k=1}^{p} \lambda_{Tx}^{k} d_{Rx}\left[\mathbf{x}+\mathbf{u}\left(\mathbf{x},\theta_{k}\right)\middle|\Psi_{i,k}, I\left(\mathbf{x},\theta_{i,k}\right)\right]. \qquad (19)$$

Note that λ_{Tx}^{k} will in general be different from λ_{Rx}^{k}, the time spent in respiratory phases during each radiation fraction. The delivered 4-D dose, summed over each i of N fractions, is given by:

$$D_{Tx} = \sum_{\text{Fraction } i=1}^{N} \sum_{\text{Phase } k=1}^{p} \lambda_{Tx}^{i,k} d_{Rx}^{i,k}\left[\mathbf{x}+\mathbf{u}\left(\mathbf{x},\theta_{k}\right)_{i}\middle|\Psi_{i,k}, I\left(\mathbf{x},\theta_{i,k}\right)\right].$$

Treatment scenario: No explicit motion management method

A clinically implemented treatment scenario (Shih et al. 2004; Starkschall et al. 2004) is to use 4-D CT for tumor spatial and temporal localization and to create a treatment plan that includes the observed tumor motion, as well as other errors such as expected variations in tumor motion, size and shape during therapy, and setup error (ICRU 1999). However there is no respiratory motion management during treatment delivery. In this case, the fluence is independent of treatment fraction and respiratory phase (i.e., $\Psi(t) \rightarrow \Psi$) and, thus, Equation (17) becomes:

$$D_{Rx} = \sum_{\text{Phase } k=1}^{p} \lambda_{Rx}^{k} d_{Rx}\left[\mathbf{x} + \mathbf{u}\left(\mathbf{x}, \theta_k\right) \middle| \Psi, I\left(\mathbf{x}, \theta_k\right)\right] . \qquad (21)$$

Given the limitation of current planning systems, Equation (21), in the current planning of these treatments, the dose calculation is generally computed on a single CT image set without deformable image registration.

Motion inclusive treatment

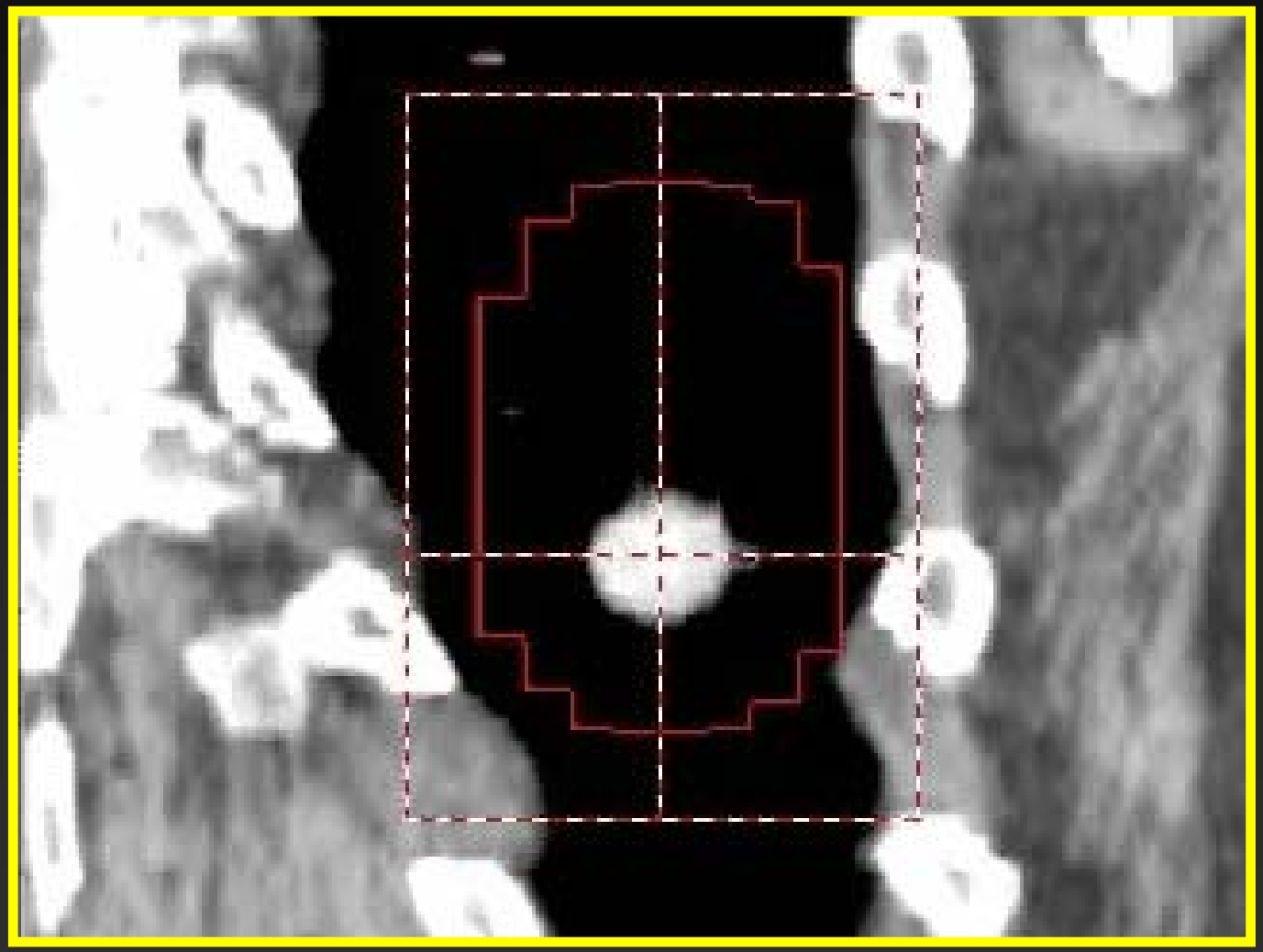

Treatment scenario: Respiratory gating

Respiratory gating involves the temporal synchronization of the radiation beam-on/off signal with a respiratory signal. Beam-on only occurs for a certain number of respiratory cycle parts. Also, the beam fluence typically is independent of respiratory phase while the beam is on (i.e., $\Psi(t) \rightarrow \Psi$) and, thus, Equation (17) becomes:

$$D_{Rx} = \sum_{\text{Phase } k=1}^{P} H(k)\,\lambda_{Rx}^{k} d_{Rx}\left[\mathbf{x}+\mathbf{u}(\mathbf{x},\theta_k)\middle|\Psi, I(\mathbf{x},\theta_k)\right], \qquad (22)$$

where $H(k)$ is the heavyside function and equals 1 for phases within the gating window and 0 otherwise. Also, λ_{Rx}^{k} is the fraction of time spent in each respiratory phase during beam-on.

Respiratory gated

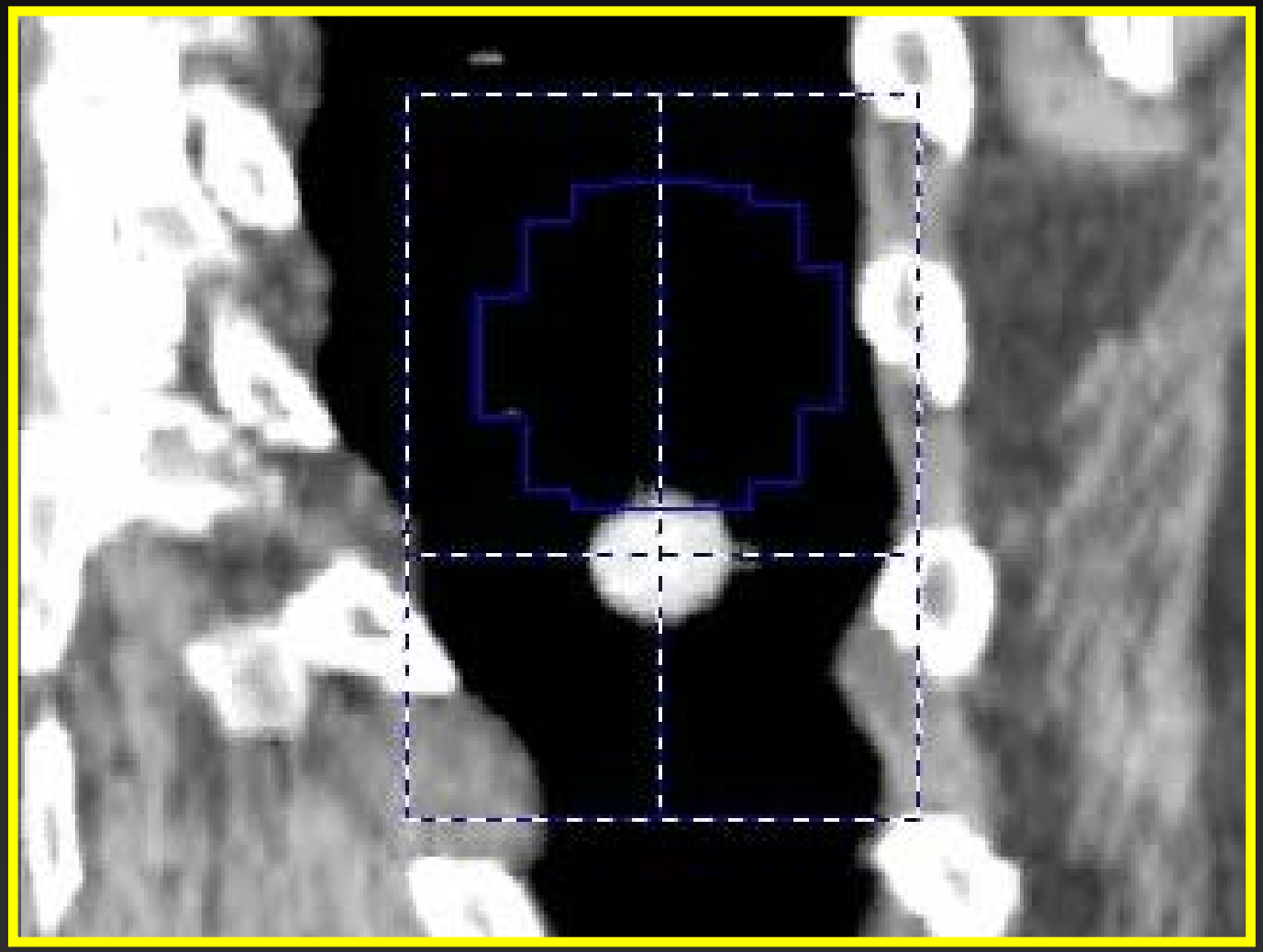

Treatment scenario: Dynamic motion compensation

$$D_{Rx} = \sum_{\text{Phase } k=1}^{P} \lambda_{Rx}^{k} d_{Rx}\left[\mathbf{x} + \mathbf{u}(\mathbf{x}, \theta_k) \middle| \Psi_k, I(\mathbf{x}, \theta_k)\right],$$

Dynamic compensation

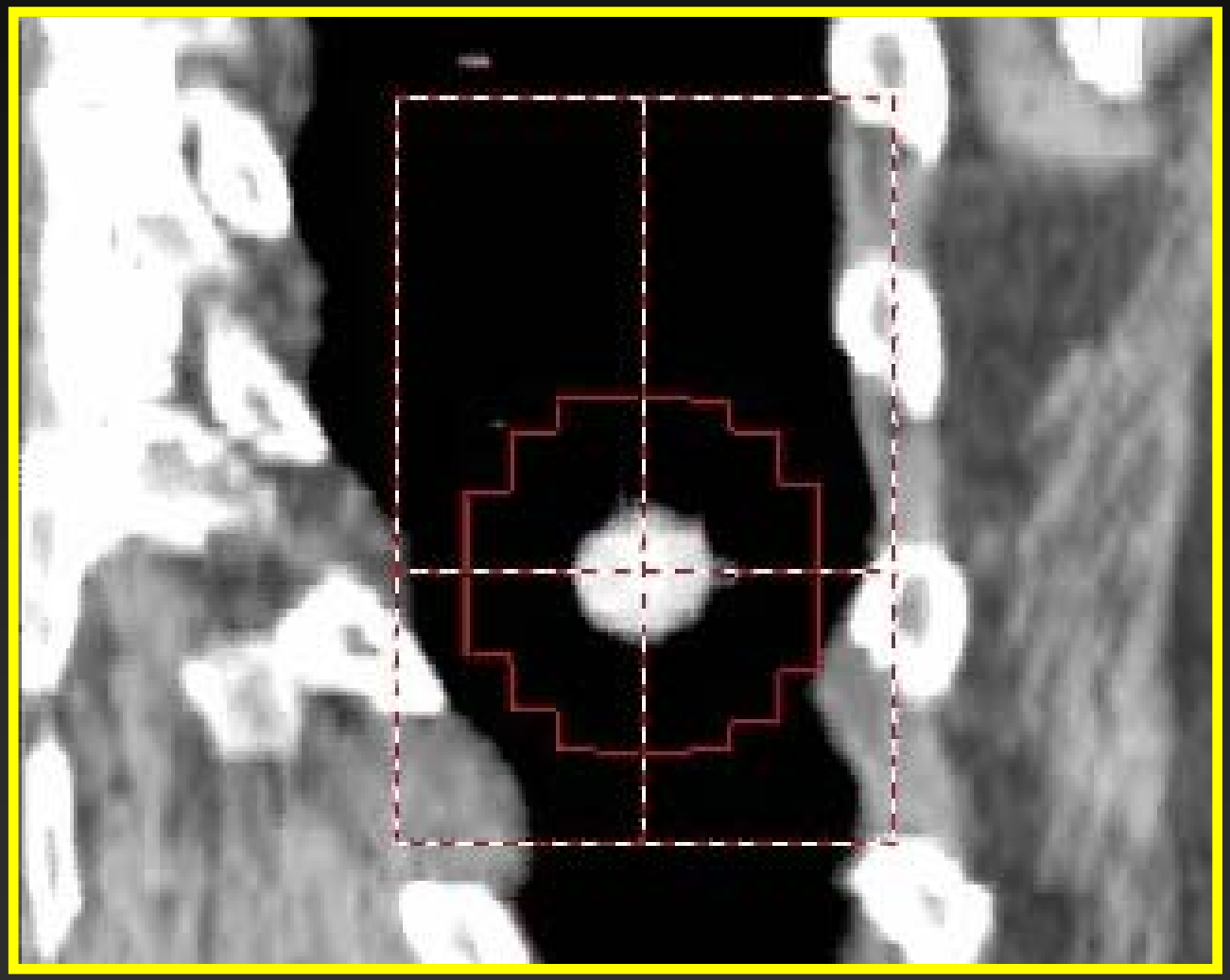

Summary and future directions

Current and future developments

- Audio-visual biofeedback
  - George *et al* Med Phys 2005, IJROBP 2006
- Respiratory signal-conditioned acquisition
  - Vedam *et al* ASTRO 2005
- 5DF breathing motion model
  - Low *et al* IJROBP 2005
- Ventilation assessment
  - Guerrero *et al* IJROBP 2005, PMB 2006
- 4D MC calculations
  - Rosu, Heath, Paganetti, Keall, Siebers …
- 4D CBCT MC calculations
  - HU errors cause both material and density errors

Summary

- Monte Carlo dose calculation has recently seen a resurgence of interest
  - Summer School and other MC workshops
  - AAPM Task Group report
  - Develop, user and vendor progress
- The acquisition and use of 4D data sets during therapy is rapidly advancing
  - Better input data to MC algorithms
- The increased accuracy offered by Monte Carlo and the increased geometric fidelity offered by 4D imaging techniques will allow treatment capabilities and clinical outcome data of unsurpassed quality

Thanks to:

- NCI R01 CA93626
- Lei Dong
- Mirek Fatyga
- Sarang Joshi
- Radhe Mohan
- Devon Murphy
- Martin Murphy
- Jeffrey Siebers
- Krishni Wijesooriya
- Jeffrey Williamson